Annals of Nuclear Energy 199 (2024) 110372

Contents lists available at ScienceDirect

Annals of Nuclear Energy

journal homepage: www.elsevier.com/locate/anucene

Comparative study of flow and heat transfer characteristics of HCF rod bundles in rectangular and triangular arrangement

Renwei Tang [a], Hangbin Zhao [a,b,*], Nailiang Zhuang [b,c], Xiaobin Tang [b,c,*]

[a] College of Astronautics, Nanjing University of Aeronautics and Astronautics, Nanjing 211106, China
[b] Key Laboratory of Nuclear Technology Application and Radiation Protection in Astronautics, Ministry of Industry and Information Technology, Nanjing 211106, China
[c] Department of Nuclear Science and Technology, Nanjing University of Aeronautics and Astronautics, Nanjing 211106, China

ARTICLE INFO

Keywords:
Helical cruciform fuel
Nuclear thermal propulsion
Flow and heat transfer characteristic
Transverse flow
Rectangular and triangular arrangement

ABSTRACT

Helical cruciform fuel (HCF) has high surface-to-volume ratio and excellent mixing performance, which can be used to form the reactor core of the nuclear thermal propulsion (NTP) system. In this research, the flow and heat transfer characteristics of HCF rod bundles in rectangular and triangular arrangement were comparatively studied by numerical simulation method. The flow resistance coefficient and heat transfer coefficient of the bundle were calculated, and the transverse flow rate between the sub-channels were analyzed. The results show that the resistance coefficient of the HCF rod bundle in triangular arrangement is larger. The transverse flow intensity in the sub-channel in triangular arrangement is 27 % larger than that in rectangular arrangement. Moreover, the maximum of J_F factor in rectangular arrangement is 1.6 % higher than that in triangular arrangement, and the minimum of J_F factor in rectangular arrangement is 11 % lower than that in triangular arrangement.

1. Introduction

With the development of space career to deep space, new requirements have been put forward for deeper space exploration, more frequent navigation missions and higher speed space navigation. NTP system with large specific impulse, long life and high stability has great prospects in future space missions. Since 1950s, the United States and the Soviet Union had successively started the research on space nuclear thermal propulsion technology. The NERVA (Palomares et al., 2020) program and the SNTP program led by the United States developed a hexagonal prism reactor with 19 working fluid channels and a particle bed reactor, which achieved abundant research results. Different from the design of the United States, USSR's RD-0410 (Gabrielli and Herdrich, 2015) reactor adopted a modular core design and used ribbon fuel, which increased the heat transfer area and enhanced the heat transfer efficiency. On this basis, HCF were proposed, which has a cruciform section and gradually twists along the axial direction (Ageenkov et al., 2002). This structure could increase the power output under the condition of the same heat flux due to its large surface-to-volume ratio. The helical structure of HCF also can increase the mixing of transverse flow; which is beneficial to make the temperature distribution in the core uniform (Malone et al., 2012). Each HCF rod can be supported by the surrounding rods, so no grid is required for HCF assembly.

Conboy et al. (2013, 2014) et al. investigated the flow characteristics of HCF rod bundle in 4 × 4 rectangular arrangement. It was found that the pressure loss of HCF rod bundle is independent of the twist pitch in the range of 50 cm to 200 cm. What's more, the tracer method was used to study the sub-channel mixing, and the effective mixing factor was obtained with the help of the sub-channel code, which was found to be related to the twist angle of HCF. Zhao et al. (2022) et al. investigated the transverse flow and turbulent mixing of a 4 × 4 HCF rod bundle. The results showed that the helical structure of the HCF rod could effectively enhance the transverse flow in the fuel bundle. Xiao et al. (2021) et al. analyzed the flow field in HCF rod bundles from the perspective of sub-channel method, and proposed a flow sweep mixing model, which was implemented in CTF code. Zhang et al. (2022) et al. compared the hydrothermal properties of HCF and wire-wrapped fuel, and the results showed that the HCF had better comprehensive performance. Therefore, HCF has great application prospects in NTP system.

At present, the study of HCF mainly focuses on the characteristics of helical structure, ignoring the effect of arrangement mode on the flow and heat transfer characteristics in the sub-channels. Jiang et al. (2023)

* Corresponding authors at: Room B305, College of Astronautics, Nanjing University of Aeronautics and Astronautics, Nanjing 211106, China (Hangbin Zhao), Room 224, Department of Nuclear Science and Technology, Nanjing University of Aeronautics and Astronautics, Nanjing, 211106, China (Xiaobin Tang).
E-mail addresses: zhaohangbin@nuaa.edu.cn (H. Zhao), tangxiaobin@nuaa.edu.cn (X. Tang).

https://doi.org/10.1016/j.anucene.2024.110372
Received 31 October 2023; Received in revised form 20 December 2023; Accepted 19 January 2024

studied the transverse mixing characteristics of the flow sweeping between the sub-channels of 19 fuel rods bundle in triangular arrangement. The study shows that turbulent mixing can be ignored, while transverse mixing is dominated by flow sweep. Cong et al. (2023) et al. used a combination of experimental and numerical simulation methods to study the transverse mixing characteristics of single-phase flows in a 5 × 5 HCF rods bundle in rectangular arrangement. The results show that the effective mixing coefficient of the HCF rod bundle is independent of Reynolds number. The local transverse flow strength is highly correlated with the local gap size, but not with Reynolds number. Therefore, due to the special geometric structure of HCF, its arrangement is also an important factor to be considered when designing a reactor.

The propellant and coolant used in the NTP system is hydrogen because of its low atomic weight. Han et al. (2022) et al carried out secondary development of the existing system analysis code applying to PWR. The physical property model, heat transfer and resistance formula of hydrogen were added into the system code. Fang et al. (2021) et al. conducted a numerical study on the hydrodynamic performance of high-temperature hydrogen flowing through 2 × 2 HCF channel, and the results showed that the relative error between the computational result and experimental result is less than 20 %.

Currently, there are few studies on the flow and heat transfer of hydrogen in HCF channel, and the influence of HCF arrangement on the flow and heat transfer process has also not been involved. Therefore, based on the numerical method, the flow and heat transfer characteristics in the HCF rod bundles in rectangular and triangular arrangement will be comparatively studied in this paper.

2. Numerical model

2.1. Geometry and grid model

The geometric structure of the HCF rod in this study is the same as that in Ref. Fang et al. (2021), and is shown in Fig. 1. The cross section of HCF rod is in the shape of cruciform, and the radius of convex and concave part is 1.5 mm. The cross section gradually twists along the axis, and the twist pitch of the rod is 500 mm. The twist pitch H, twist angle α and axial distance z satisfy $\alpha = 360^\circ \cdot z/H$. The structures of the fuel rod bundles in rectangular arrangement and in triangular arrangement are shown in Fig. 2.

Because the fuel rod structure is periodic in the length direction, only one twist pitch of computational domain is selected for calculation, so that the computational cost can be reduced. For rectangular arrangement, 3 × 3 fuel rod bundles are adopted, and for triangular arrangement, 7 fuel rod bundles are adopted. The fluid domains of these two bundles are shown in Fig. 3. In order to improve the grid quality, it is assumed that there is a 0.4 mm gap between the adjacent fuel rod. The same treatment has been adopted in other studies (Zhao et al., 2017; Liu et al., 2017), which has little effect on the result. Grids of these two fluid domains are shown in the Fig. 4. The grids in the regions near the fuel rod surface are refined, because the velocity gradient and temperature gradient in these regions are large. With the distance to the fuel rod surface increasing, the grid size also increases proportionally. All grids are hexahedral volume grids or square surface grids. The minimum of the grid quality is greater than 0.4, and the average grid quality is greater than 0.73.

In order to investigate the effect of grid density on the result, three types of grids with different densities are generated. The total numbers of these three types of grids and the corresponding pressure drops from inlet to outlet calculated are shown in Table 1. Fig. 5 shows the variations of axial pressure drop of the HCF rod bundles when total grids number increases. When the number of grids is greater than that of medium density, the change of the axial pressure drop distribution is so small that the grid effect can be ignored. The maximum difference between the pressure drop calculated by medium grid type and that by fine grid type model is less than 0.12 %. Fig. 6 and Fig. 7 show the velocity distributions on the character lines in two different arrangements. The locations of the character lines are marked in red on the diagram. Whether triangular or rectangular arrangement, the velocity distribution calculated by medium grid type are not much different from those by fine grid type. Consequently, the medium density mesh model is

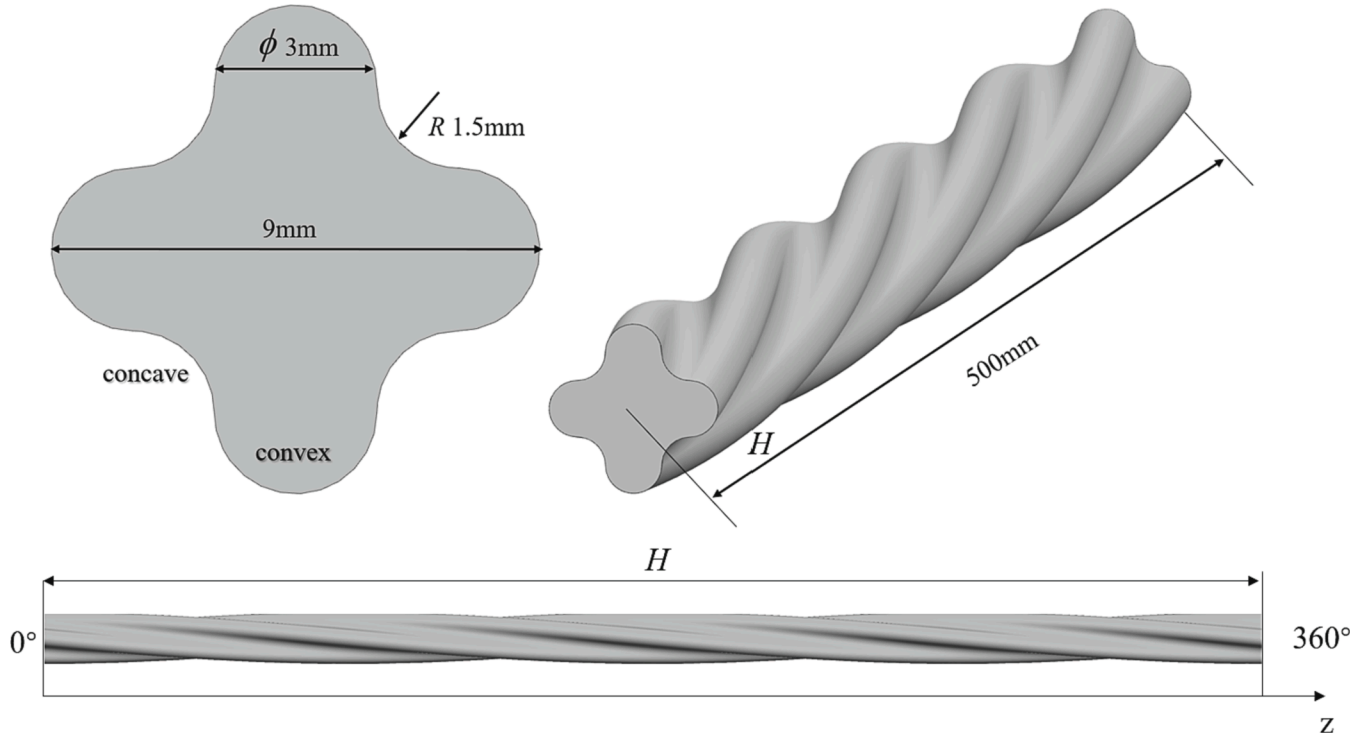

Fig. 1. HCF rod.

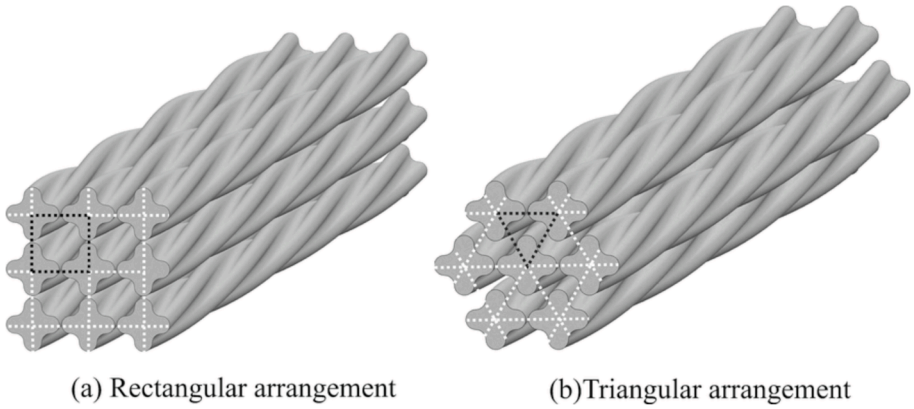

Fig. 2. Structure of fuel rod bundles in two arrangements.

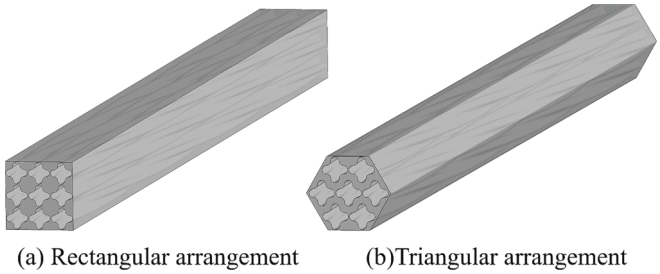

Fig. 3. Fluid domain.

adopted in the following calculations.

2.2. Governing equation

The governing equations of mass, momentum, and energy are respectively shown as follows:

Mass equation,

$$\nabla\cdot(\rho\vec{v})=0 \tag{1}$$

Momentum equation

$$\nabla\cdot(\rho\vec{v}\vec{v})=-\nabla p+\nabla\cdot(\bar{\bar{\tau}})+\rho\vec{g}+\vec{F} \tag{2}$$

Where

$$\bar{\bar{\tau}}=\mu\left[(\nabla\vec{v}+\nabla\vec{v}^{T})-\frac{2}{3}\nabla\cdot\vec{v}\cdot\vec{I}\right] \tag{3}$$

Energy equation,

Table 1
Effect of grids number.

Grid types	Rectangular arrangement		Triangular arrangement	
	Grids number (millions)	Pressure drops (Pa)	Grids number (millions)	Pressure drops (Pa)
Coarse (1)	417	17,870	418	22,280
Medium (2)	718	18,940	655	23,330
Fine (3)	849	18,950	786	23,360

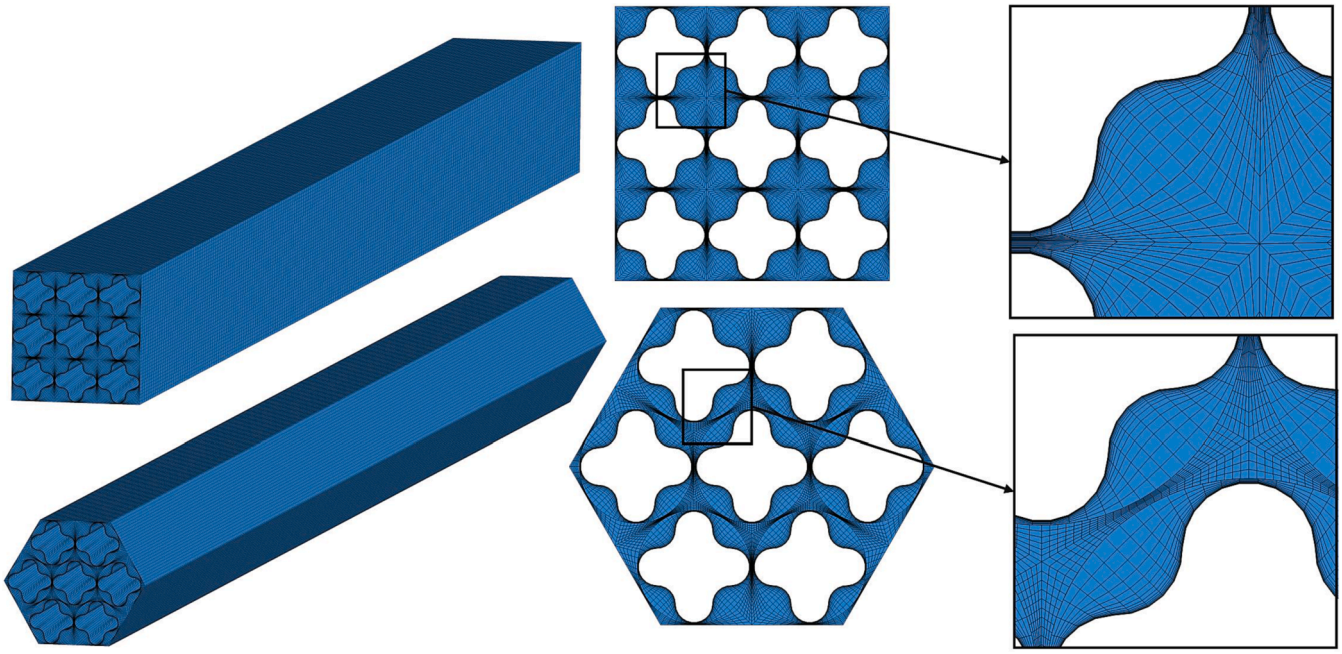

Fig. 4. Fluid domain mesh.

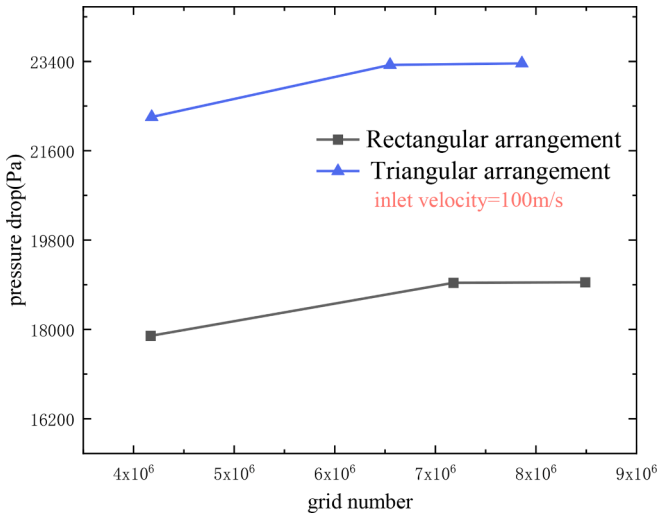

Fig. 5. Effect of grids number.

$$\nabla\cdot\left[\rho\vec{v}\left(h+\frac{v^2}{2}\right)\right]=\nabla\cdot\left(k_{eff}\nabla T-\sum_j h_j\vec{J}_j+\overline{\overline{\tau_{eff}}}\cdot\vec{v}\right)+S_h \tag{4}$$

Where, $k_{eff}=k+k_{turb}$,which the turbulence effect enhances the heat transfer effect.

Based on the research conclusion of Ref. (Fang et al., 2021), SST k-ω model is more accurate, reliable and suitable for adverse pressure gradient flow, compressibility, shear flow diffusion and transonic shock wave, incorporating modification for low Reynolds number effects, compressibility, and shear flow propagation. Therefore, SST k-ω is adopted as the turbulence model. The turbulent kinetic energy, k and specific dissipation rate, ω, can be obtained from the following transport equation:

$$\frac{\partial}{\partial t}(\rho k)+\frac{\partial}{\partial x_i}(\rho k u_i)=\frac{\partial}{\partial x_i}\left[\left(\mu+\frac{\mu_t}{\sigma_k}\right)\frac{\partial k}{\partial x_i}\right]+G_k-Y_k+S_k+G_b \tag{5}$$

$$\frac{\partial}{\partial t}(\rho\omega)+\frac{\partial}{\partial x_i}(\rho\omega u_i)=\frac{\partial}{\partial x_i}\left[\left(\mu+\frac{\mu_t}{\sigma_\omega}\right)\frac{\partial\omega}{\partial x_i}\right]+G_\omega-Y_\omega+S_\omega+G_{\omega b} \tag{6}$$

Where, G_k is the turbulent kinetic energy generated by the average

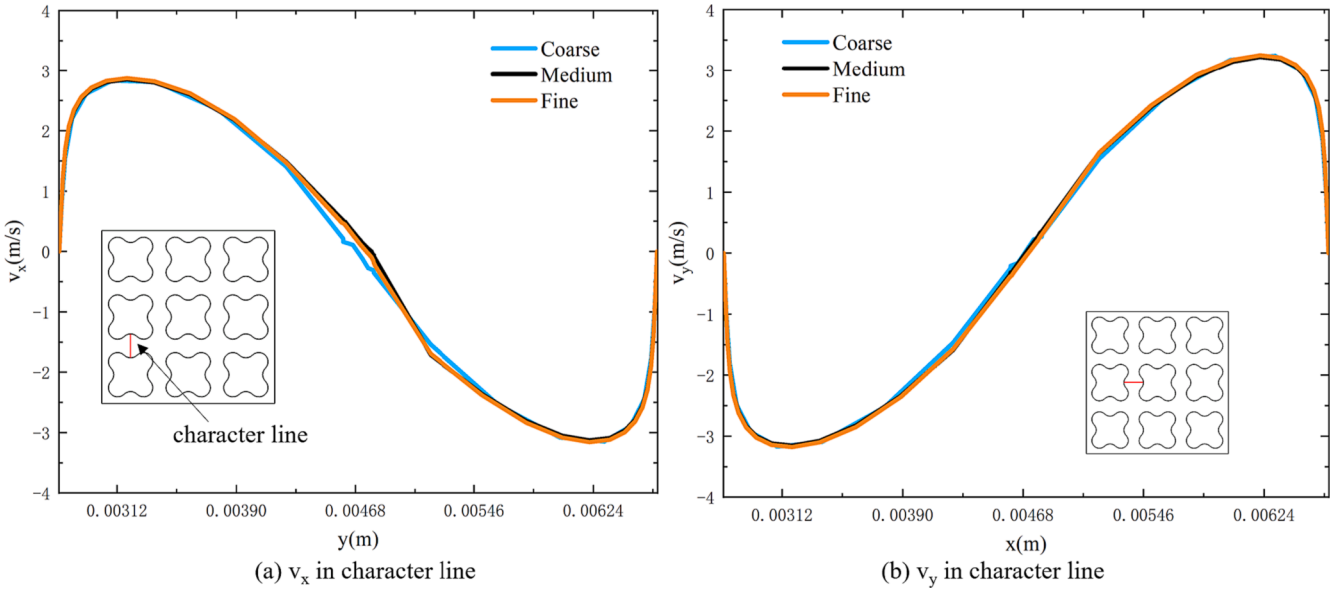

(a) v_x in character line (b) v_y in character line

Fig. 6. Velocity distribution on the characteristic line in rectangular arrangement.

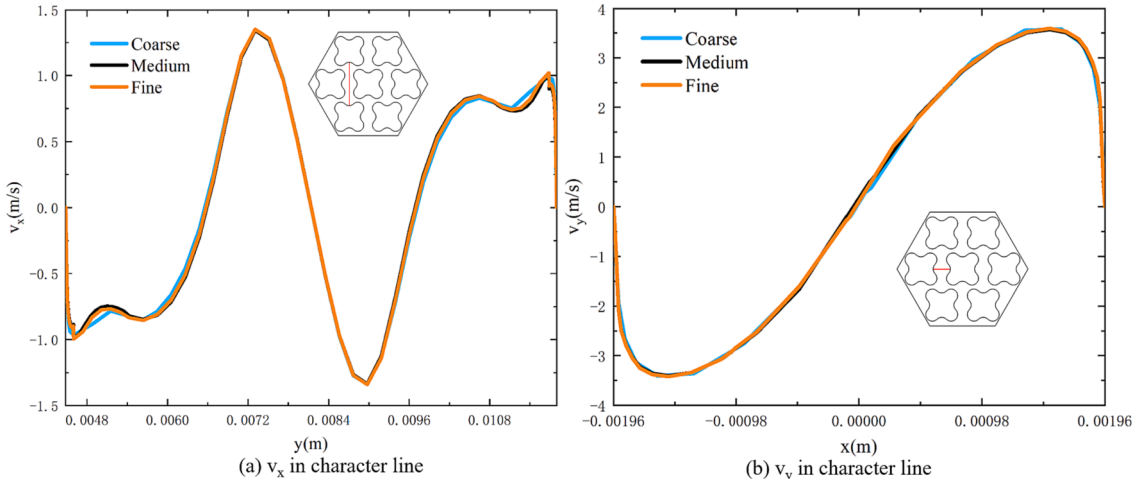

(a) v_x in character line (b) v_y in character line

Fig. 7. Velocity distribution on the characteristic line in triangular arrangement.

velocity gradient. G_ω represents the formation of ω. μ_t is the turbulent viscosity. σ_k and σ_ω are the turbulent Prandtl numbers for k and ω. Y_k and Y_ω represent the dissipation of k and ω due to turbulence. S_k and S_ω are user-defined source terms. G_b and $G_{\omega b}$ explain the buoyancy terms described in the effects of buoyancy on turbulence in the k-ω model.

2.3. Boundary condition and solving method

In this study, the flow and heat transfer characteristics of HCF rod bundles in rectangular and triangular arrangement are comparatively studied by numerical simulation method. The boundary conditions are listed in Table 2. The inlet boundary condition of channel is defined as velocity inlet and the outlet boundary condition is defined as pressure outlet. The inlet velocity varies between 50 m/s and 150 m/s and the inlet temperature is 300 K. The outlet pressure is 6.0 MPa. The uniform heat flux, 5.0 MW/m^2, is imposed on the surface of the HCF rod. The wall of the bundle channel is defined as no slip boundary condition, and the adiabatic boundary condition is imposed on the hexagonal duct wall.

The pressure–velocity couple is adopted for SIMPLE scheme. The governing equations are discretized by second-order upwind method. The convergence criterion of continuity, momentum and energy are 10^{-6}. Finally, the calculation is performed with ANSYS FLUENT.

NASA Lewis Research Center carried out many experiments on the heat transfer characteristics of hydrogen for propulsion. The experimental results (Taylor, 1970) that hydrogen gas flows through an electrically heated tungsten tube with a length-to-diameter ratio of 77 and an inner diameter of 2.95 mm are introduced for model validation. Fig. 8 shows that the hydrogen temperature obtained from this model is in good agreement with the experiment.

3. Results and discussion

3.1. Resistance characteristic analysis

Fig. 9 shows the streamline of working medium in flow channel of HCF rod bundles in two arrangements. It can be seen that the fluid flows along the helical structure of the fuel rod, and vortex occurs in the center of the sub-channel. Fig. 10 shows the pressure distribution in the flow channel. The pressure gradually decreases linearly with the increase of the distance to inlet, and the pressure drop from inlet to outlet in the flow channel increases with the increase of the inlet speed. In addition, the pressure drop of the rod bundle in triangular arrangement is greater than that in the rectangular arrangement.

The frictional coefficient of the bundle is calculated as follows:

$$\Delta p = 4f\frac{L}{D}\frac{G^2}{2\rho} \tag{7}$$

Where Δp represents pressure drop, f represents resistance coefficient, L represents flow channel length, D represents hydraulic diameter, G represents mass flow rate, and ρ represents density.

The resistance coefficients are shown in Fig. 11. The calculation results are in good agreement with Koo model, and the relative error is within 5 %. The empirical formula of Koo model (Han et al., 2022) is as follows:

$$f = 0.0014 + 0.125/\mathrm{Re}^{0.32} \tag{8}$$

Table 2
Boundary conditions.

Parameters	Value
Outlet pressure (MPa)	6.0
Inlet temperature (K)	300
Inlet velocity (m/s)	50 ~ 150
Heat flux (MW/m^2)	5.0

Where Re is Reynolds number. The results show that the friction resistance of rod bundle in triangular arrangement is greater than that in rectangular arrangement when the inlet velocity is the same, because the structure of triangular arrangement is more compact and the hydraulic diameter is smaller.

3.2. Transverse flow characteristic analysis

Fig. 12 shows the relationship between twist angle and axial distance. H is the twist pitch of the fuel rod, and the relative position z/H determines the twist angle of the fuel rod, and when z/H = 1, the twist angle of the fuel rod is 360°. Fig. 13 and Fig. 14 shows the velocity vector distributions in different cross sections of the bundles. It can be seen that the fluid will be disturbed by its concave and convex parts due to the helical structure, which enhance its transverse mixing ability. Around the fuel rod, the fluid flows clockwise around the center of the fuel rod. At the same time, due to the near-wall swirl, the fluid flows counterclockwise at the center of the sub-channel.

For the rectangular arrangement, z/H = 5/8 is the position where the fuel rod has rotated 225°, and then the fuel rod rotates another 45° to z/H = 3/4. As the gap between the fuel rods changes from maximum to minimum, the flow pattern of the fluid in the channel changes accordingly. At z/H = 5/8, the flow in the channel not only includes the flow in the sub-channel, but also includes the mixed flow between the sub-channels. With the increase of the twist angle, the mixed flow between the sub-channels gradually weakens. At z/H = 3/4, the flow in the channel develops into a single counterclockwise flow in the center of the sub-channel. In contrast, for the triangular arrangement, z/H = 2/3 is the position where the fuel rod has rotated 240°, and then the fuel rod rotates another 60° to the position where z/H = 5/6. As shown by the position of the red box in the Fig. 14, the position of mixed flow between sub-channels also changes with the change of twist angle.

Fig. 15 shows a simplified flow diagram of the fluid in the channels in two different arrangements. At the fuel rod gap, the flow direction is bidirectional, while at the channel edge, the flow direction is unidirectional.

The names of the sub-channel and HCF rod in the numerical model are shown in Fig. 15. Because of the central symmetry of the structure, the flow characteristics of the sub-channel are similar, so the A32 and B34 sub-channels are selected respectively for analysis and research of the flow channels in two arrangements. A31-A32 is defined as the interface of sub-channels A31 and A32. Therefore, A31-A32 and A32-A42 are the interfaces between the center sub-channel and the edge sub-channel in the flow channel, and A22-A32 and A32-A33 are the interfaces between the center sub-channels in the flow channel. Similarly, B34-B43 is the interface between the center sub-channel and the edge sub-channel in the flow channel, and B33-B34 and B34-B35 are the interfaces between the center sub-channels in the flow channel.

The Fig. 16 shows the velocity contours in y direction on the interface A32-A42 and interface B34-B43. The left side is the inlet direction and the right side is the outlet direction. It can be seen that the gap width between the adjacent fuel rods varies periodically. In combination with Fig. 15, the velocity distribution is symmetrical about the centerline and the direction of velocity is opposite.

Based on above discussion, the flow on the interface between two sub-channels can be divided into positive and negative direction. The positive and negative transverse flow rate on the interface are defined as follows:

$$G^+ = \int v^+ dl \tag{9}$$

$$G^- = \int v^- dl \tag{10}$$

where v^+ and v^- are positive and negative velocities respectively on the

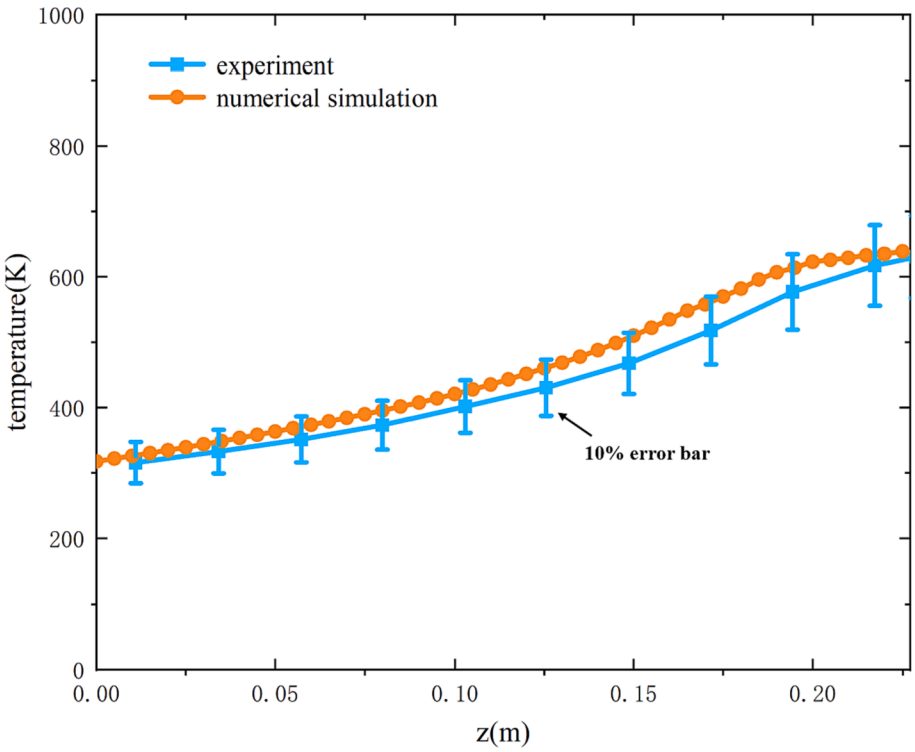

Fig. 8. Temperature distribution obtained from numerical simulation and experiment.

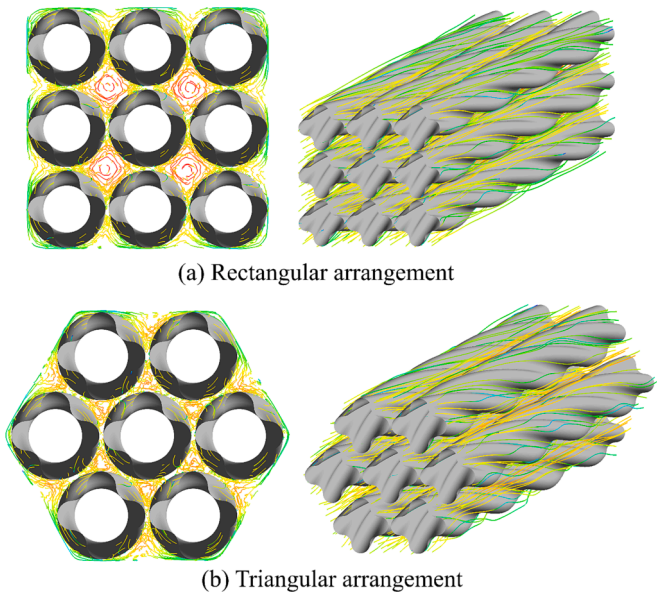

Fig. 9. Streamline of channel in two arrangements.

interface. G^+ and G^- represent line integrals of positive and negative velocities respectively.

Fig. 17 and Fig. 18 show the variations of transverse flow rate on interfaces around sub-channel A32 and sub-channel B34 along axial direction. As can be seen, the flow between the sub-channels shows obvious periodicity, which is caused by the twist structure of the HCF. The number in front of the legend represents the inlet velocity.

As shown in the Fig. 17, due to the central symmetry of the arrangement, the transverse flow rate distributions on interface A31-A32 and A32-A42 are similar, and the same phenomenon can be observed on interface A22-A32 and A32-A33 as well. Fig. 17(a) and Fig. 17(h), Fig. 17(b) and Fig. 17(g) are symmetric about the x-axis, that is to say, the velocity in the x and y directions is switched and reversed. The v_x is defined as transverse flow rate in x direction. And the v_x on interface A31-A32 is equal to the negative of the v_y on interface A32-A42.

In addition, with the increase of the inlet velocity, the transverse flow rate also increases correspondingly. The v_x and v_y on each interface around sub-channel A32 differ by 5–10 times. For example, the v_x on the interface A31-A32 shown in Fig. 17(a) is much higher than the v_y shown in Fig. 17(b), while the v_y on interface A22-A32 shown in Fig. 17(d) is much higher than the v_x shown in Fig. 17(c). In other words, the flow between sub-channels is mainly perpendicular to the interface.

However, although the flow between sub-channels parallel to the interface does not dominate, their distribution is different from that perpendicular to the interface. Fig. 17 shows that the velocity parallel to the interface direction almost returns to zero every 45°, whose period is half of that of the velocity perpendicular to the interface. That's because the fuel rods reach their maximum or minimum spacing every 45°, which directly affects the parallel velocity. It is worth noting that the v_y on interface A31-A32 shown in Fig. 17(b) and the v_x on interface A32-A42 shown in Fig. 17(g) are a little more special. Because interface A31-A32 and interface A32-A42 are connected the center sub-channel and the edge sub-channel, they will be affected by the wall surface. Transverse flow rate perpendicular to the interface changes periodically with the twist angle, and their value becomes to the minimum every 90°.

The distribution of transverse flow rate on each interface around sub-channel B34 in triangular arrangement shown in Fig. 18 is discussed as follows. The v_x velocity distribution on the B34-B43 interface shown in Fig. 18(e) also returns to zero every 45 degrees, similar to the v_y on interface A31-A32 as shown in Fig. 17(b) and the v_x on interface A32-A41 as shown in Fig. 17(g). The transverse flow rate at other interfaces also varies periodically with the twist angle, and its value reaches the minimum every 90°. The difference is that their velocity changes are not synchronous, which have phase difference, and their peak value does not appear in the same position.

The transverse flow rate between two sub-channels is discussed

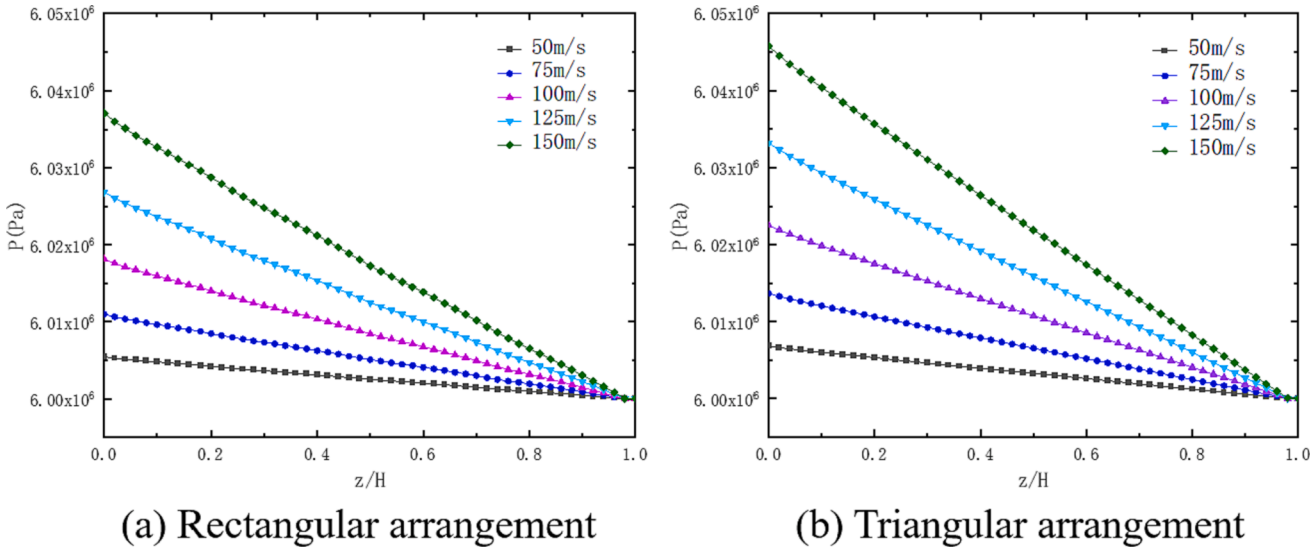

Fig. 10. Axial distribution of pressure in channel.

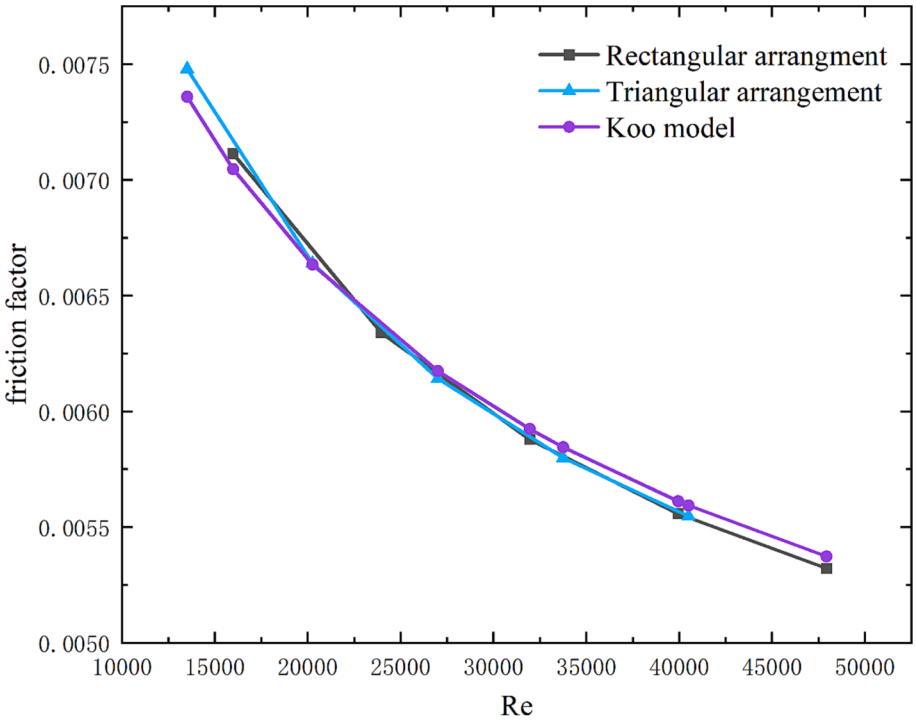

Fig. 11. Resistance coefficient and Koo model.

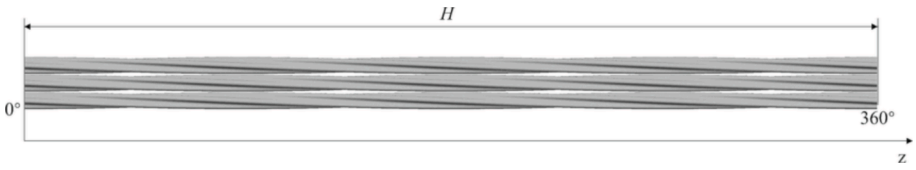

Fig. 12. Twist angle and axial distance.

above, in order to quantitatively analyze the transverse mixing effect in the channel due to the helical structure, transverse flow intensity *St* (Chen et al., 2018) is introduced and defined as follows:

$$St = \frac{\overline{v_t}}{\overline{v_z}} = \frac{\sqrt{\overline{v_x^2 + v_y^2}}}{\overline{v_z}} \tag{11}$$

Where $\_v_t$ is the average transverse velocity, and $\_v_z$ is the average axial

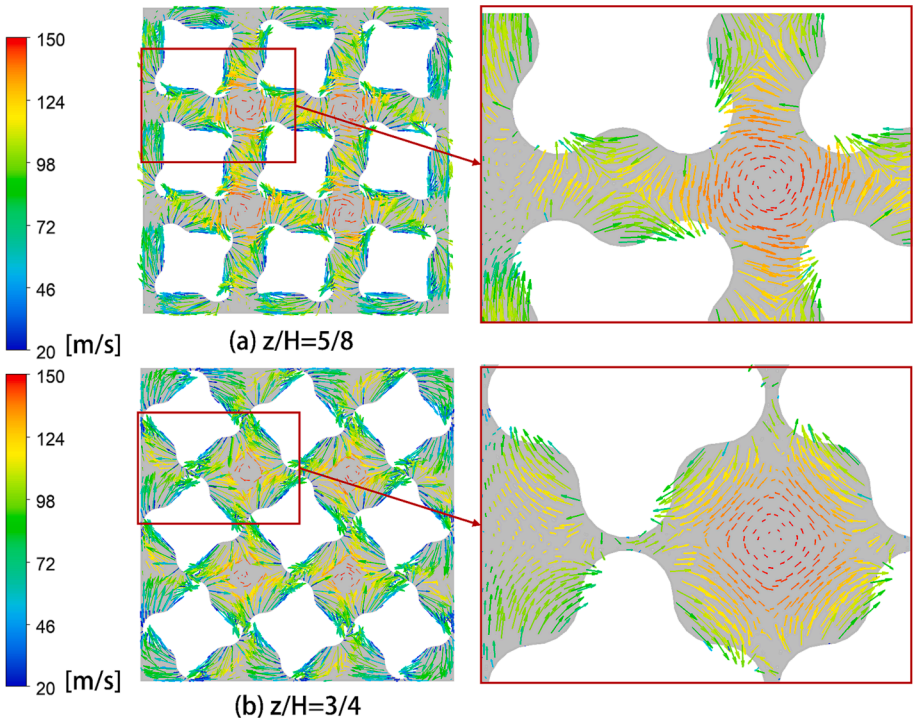

Fig. 13. Velocity vector distribution in rectangular arrangement.

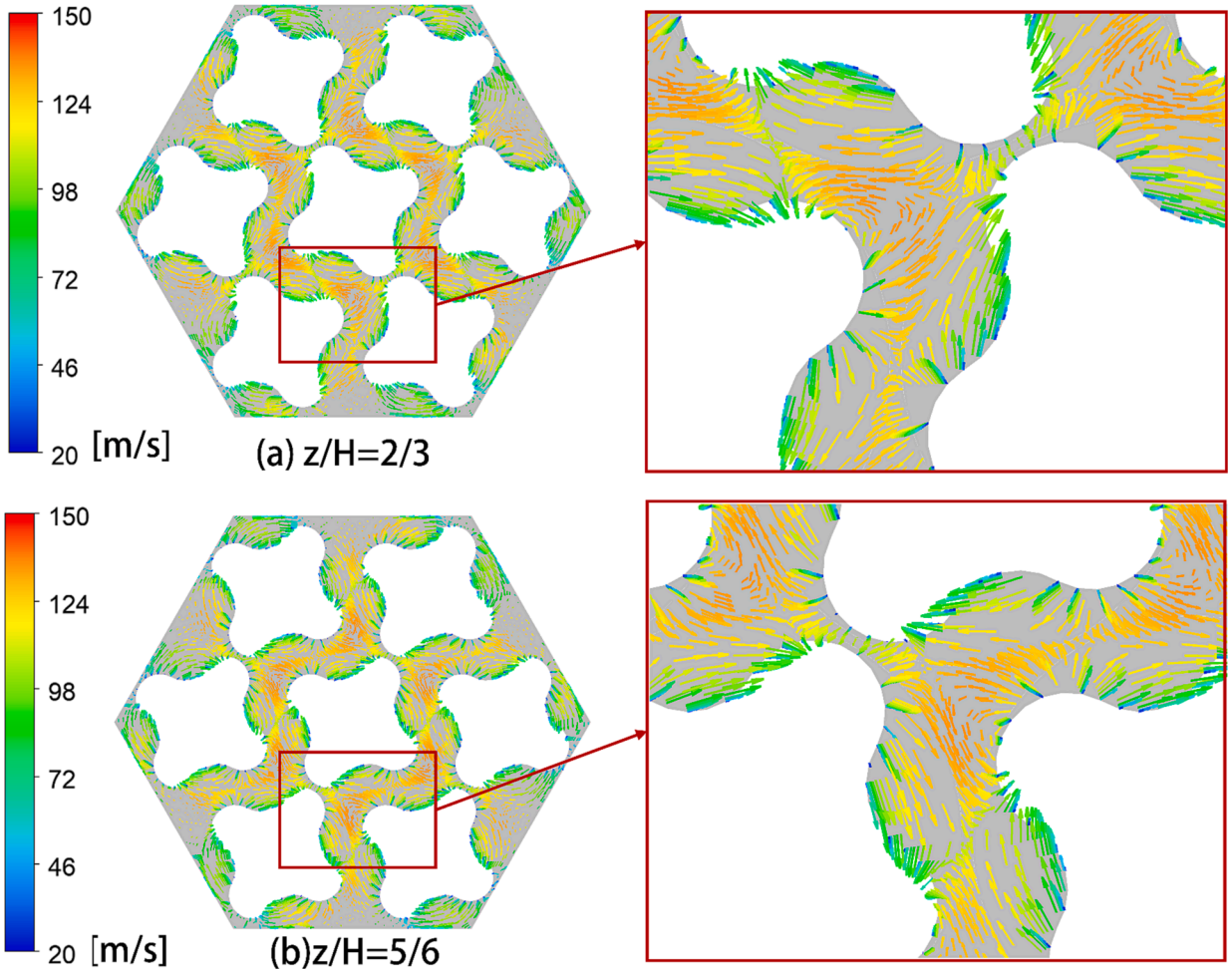

Fig. 14. Velocity vector diagram distribution in triangular arrangement.

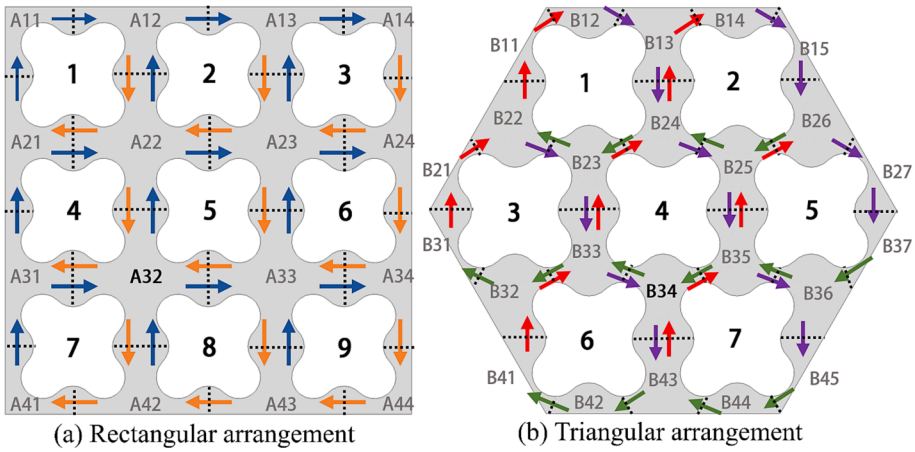

Fig. 15. Simplified flow and sub-channel diagram.

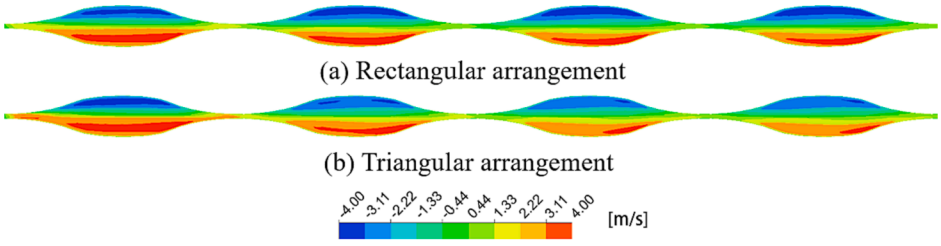

Fig. 16. Horizontal velocity contours between fuel rods.

velocity.

Fig. 19 shows the variation of the average transverse flow intensity on the interfaces around sub-channel A32 and sub-channel B34. Although the transverse flow rate at the same interface is different at different inlet velocity, the average transverse flow intensity is the same regardless of the unstable flow factors at the front of the flow channel. That is to say, the transverse flow intensity does not vary with the inlet velocity varying. It only depends on the flow path geometry. By comparing the *St* curves of the interfaces around sub-channel A32 and sub-channel B34, it can be clearly seen that the transverse flow intensities of the bundle in rectangular arrangement and in triangular arrangement change periodically. In additional, the transverse flow intensities on the interfaces around sub-channel A32 changes synchronously, while the transverse flow intensities on the interfaces around sub-channel B34 is different. There is a phase difference of 180°. Their maximum values occur at the points where the gap width is the furthest, and their minimum values occur where the gap width is the smallest. The difference between the maximum transverse flow intensities on the interfaces around sub-channel A32 and that around sub-channel B34 is no more than 3 %.

Fig. 20 shows the average transverse flow intensity in sub-channel A32 and sub-channel B34. The average transverse flow intensity in sub-channel B34 is 27 % greater than that in sub-channel A32, which means that the transverse flow intensity in triangular arrangement is stronger than that in rectangular arrangement.

3.3. Heat transfer characteristics analysis

The temperature distributions in the flow channel of HCF rod bundles in rectangular and triangular arrangements are respectively shown in the Fig. 21 and Fig. 22. It can be intuitively seen that the temperature near the rod surface is higher, and the temperature in the concave region is higher than that in the convex region. Because the heat in the concave is not easily carried away. However, due to the continuous heating of the fuel rod, with the increase of the twist angle, the high temperature area near the fuel rod is expanded. At the center of the sub-channel, which is far from the fuel rod surface, it is less affected by the near-wall swirl, and the heat transfer speed is slow.

The azimuthal wall temperature distributions of the fuel rod 5 in rectangular arrangement and the fuel rod 4 in triangular arrangement at z/H = 3/4 positions are compared in the Fig. 23. It describes that as the hydrogen flows along the axial direction, the wall temperature also presents a periodic trend due to its helical structure. The overall change trend is relatively uniform, but the temperature of the fuel rod surface changes more acutely. Fig. 23 shows that the wall temperature of fuel rod in the triangular arrangement is higher than that in the rectangular arrangement, because the rod bundle in triangular arrangement is more compact. In addition, the maximum temperature difference of the wall temperature of fuel rod in the triangular arrangement is also larger than that in the rectangular arrangement, by about 30 %.

Fig. 24 shows the average hydrogen temperature and average wall temperature in flow channel. As can be clearly seen, the average hydrogen temperature in the triangular arrangement is higher than that in the rectangular arrangement. The maximum ratios of wall temperature to hydrogen temperature in rectangular and triangular channels are 2.47 and 2.41, respectively. In addition, the wall temperature of fuel rod in rectangular arrangement has a peak value in every twist pitch, which lag a little behind the location where the minimum gap width occurs. The reason is that when the gap width is the minimum, the transverse flow intensity between the sub-channels is the lowest, and the heat from the fuel rod wall is not carried away in time. In contrast, the fuel rods in triangular arrangement does not have this phenomenon, and the overall fuel rod wall temperature gradually increases.

The dimensionless coefficient J_F is used to evaluate the overall hydraulic performance of the bundle (Saha et al., 2020) and characterize the relationship between the properties of convective fluid, heat transfer coefficient, flow conditions and geometric shape. The calculation method of J_F is given by

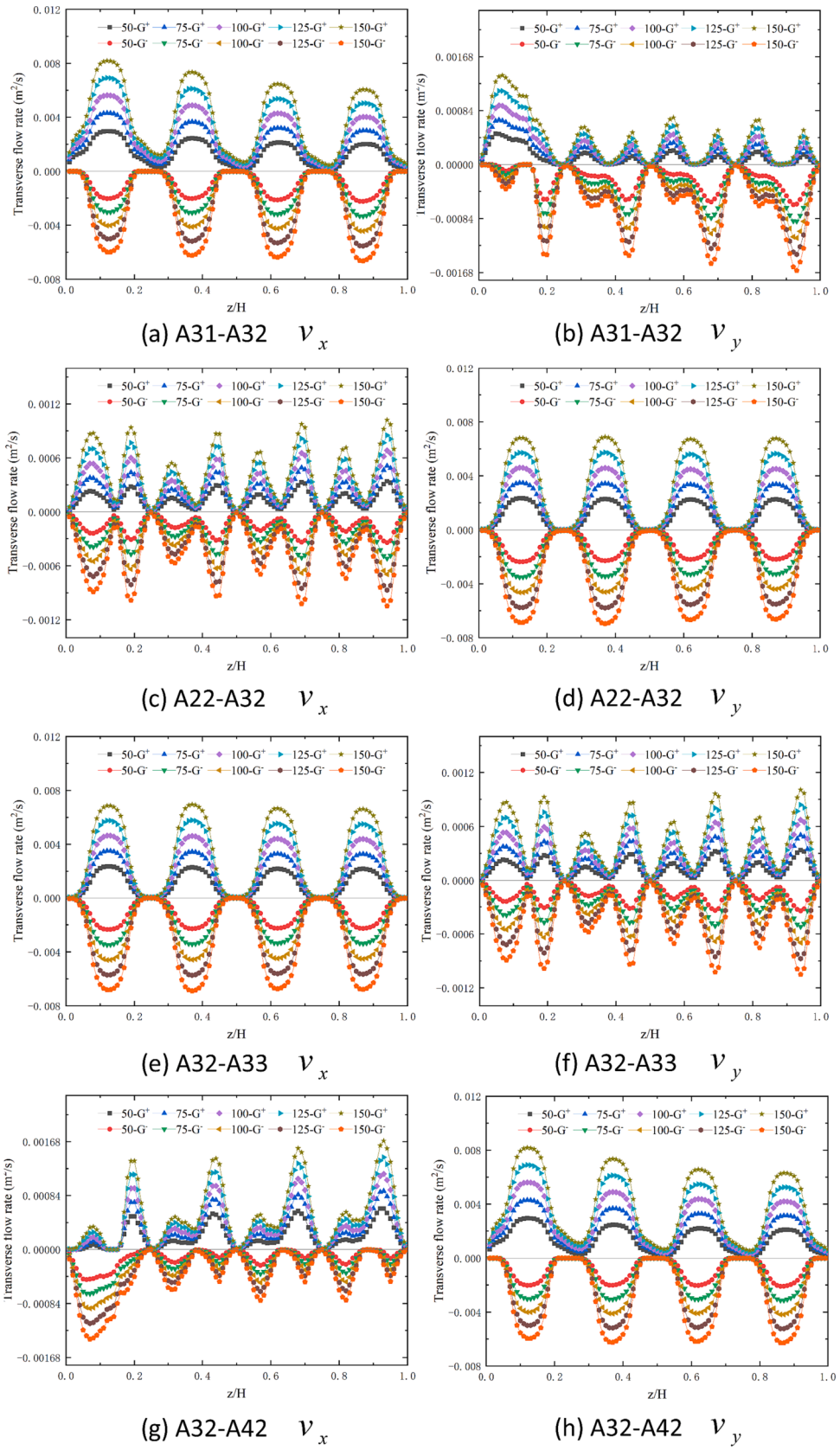

Fig. 17. The transverse flow rate on interfaces around sub-channel A32.

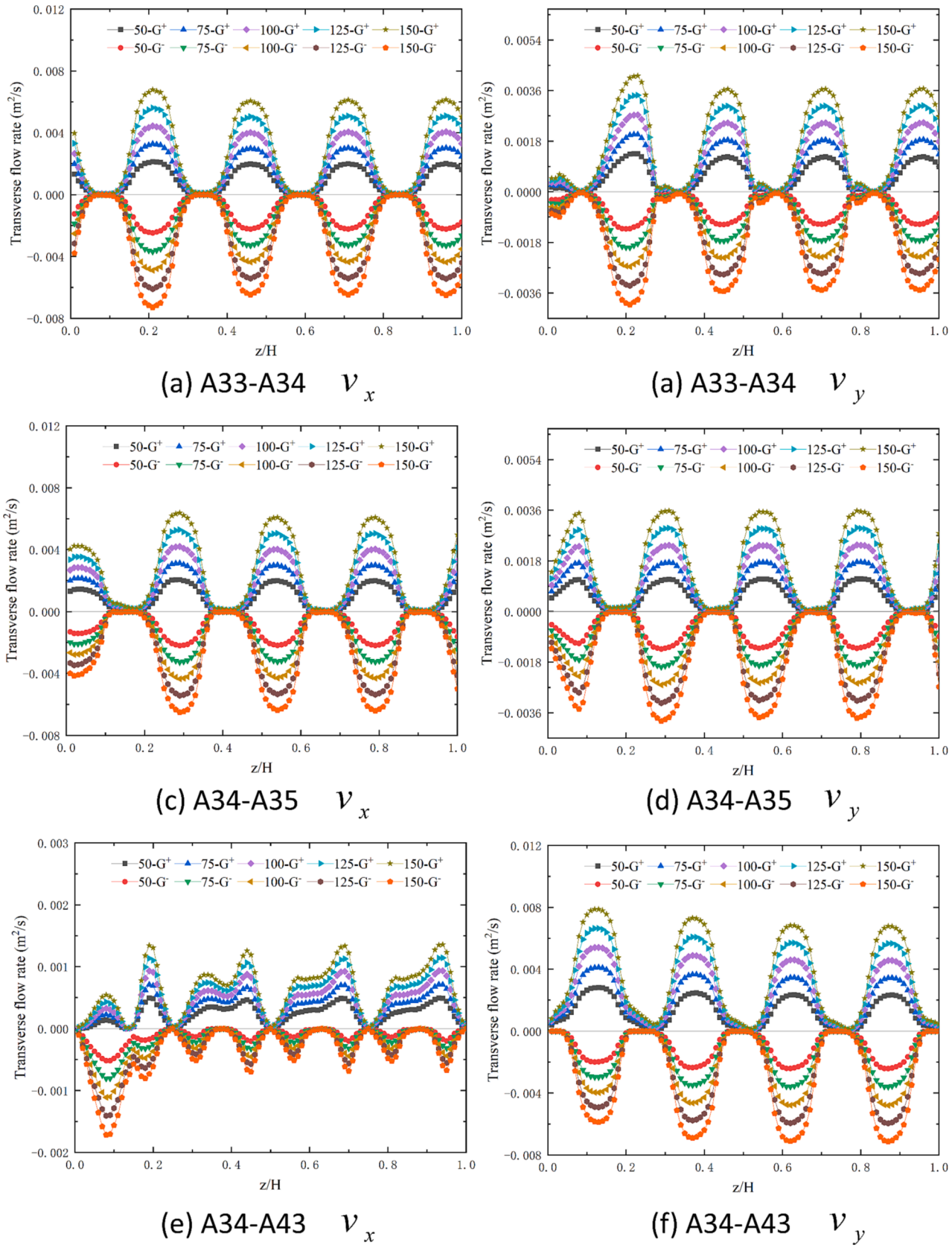

Fig. 18. The transverse flow rate on interfaces around sub-channel B34.

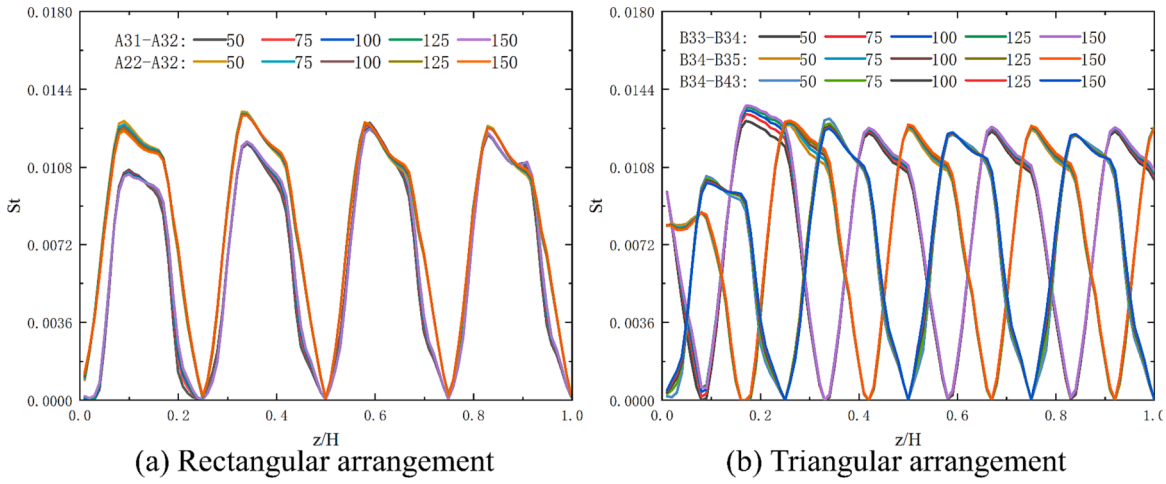

Fig. 19. Transverse flow intensity on the interfaces around sub-channel A32 and sub-channel B34.

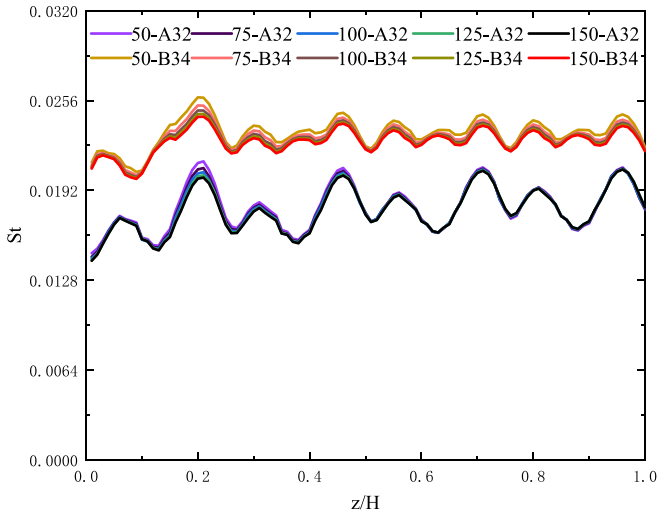

Fig. 20. Transverse flow intensity of the sub-channel.

$$J_F = \frac{j}{f^{1/3}} \tag{12}$$

$$j = \frac{Nu}{\mathrm{Re}\cdot Pr^{1/3}} \tag{13}$$

Where f represents resistance coefficient, Nu is Nusselt number, and Pr is Prandtl number.

Fig. 25 shows the variations of J_F factors of the bundles in the two arrangements. As can be seen, the J_F factor near the channel inlet gradually decreases along the axial direction. With z/H increasing, it gradually becomes stable, presenting obvious periodicity. However, the J_F factor of rod bundle in rectangular arrangement fluctuates more strongly than that in triangular arrangement. The maximum value of J_F factor in rectangular arrangement is 1.6 % higher than that in triangular arrangement, and the minimum value is 11 % lower than that in triangular arrangement.

4. Conclusion

The flow and heat transfer characteristics of HCF rod bundles in rectangular and triangular arrangement are comparatively studied in

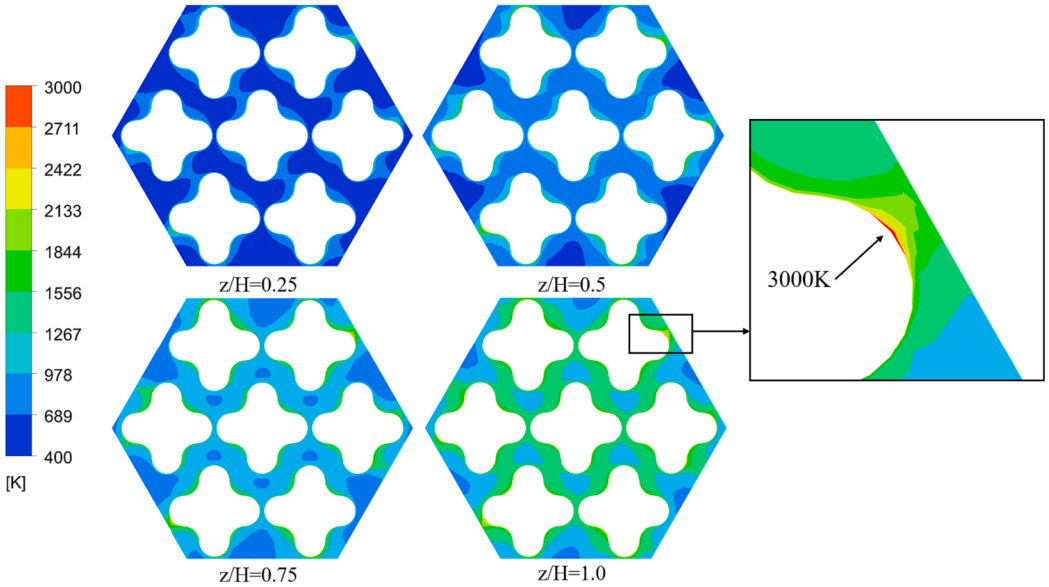

Fig. 21. Temperature distributions of different axial positions in triangular arrangement.

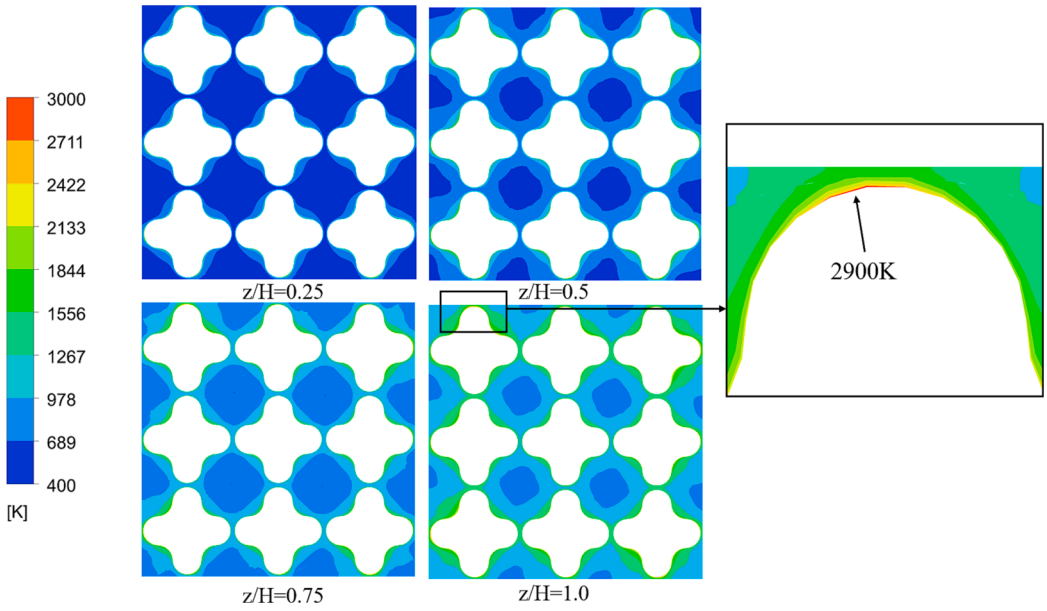

Fig. 22. Temperature distributions of different axial positions in rectangular arrangement.

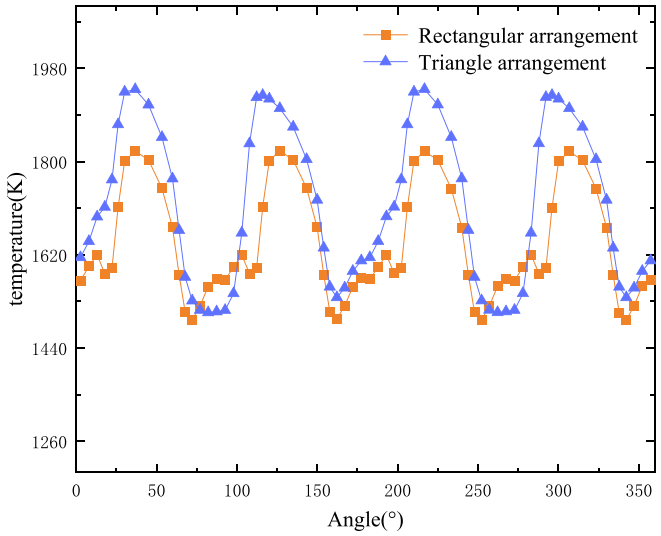

Fig. 23. Azimuthal wall temperature distributions of the fuel rod at z/H = 3/4 in two arrangements.

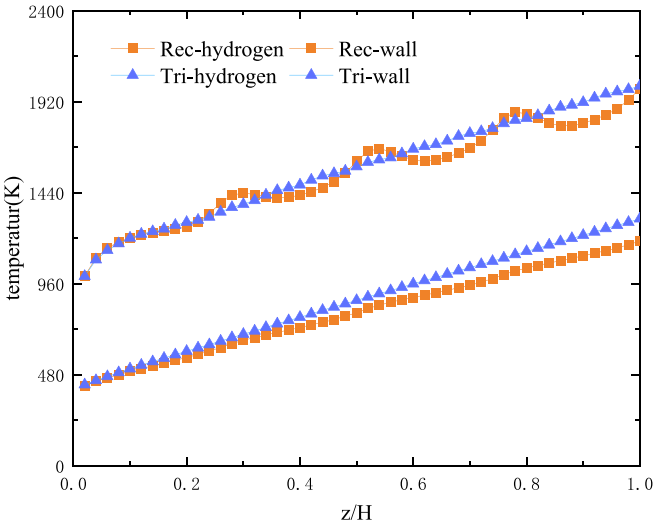

Fig. 24. Comparison of hydrogen temperature and wall temperature.

this research. The fuel rod geometry and operating conditions are the same for different arrangements. The resistance coefficient, transverse flow intensity and J_F factor of the bundle are respectively calculated and analyzed respectively under the same working condition. The following conclusions can be drawn:

(1) The flow channels of HCF rod bundle in triangular arrangement has smaller hydraulic diameter, so its resistance coefficient is greater than that in rectangular arrangement at the same inlet speed;
(2) The transverse flow intensity at each interface around sub-channel A32 and B34 varied periodically. The former changes synchronously, while the latter is not synchronous, and the phase difference is 180°. The maximum transverse flow intensity difference between the interface around sub-channels A32 and B34 is no more than 3 %, but the transverse flow intensity of channel B34 is 27 % greater than that of channel A32;
(3) The maximum wall temperature difference of fuel rod in triangular arrangement is about 30 % larger than that in rectangular arrangement when the heat flux through the fuel rod surface is equal;
(4) The maximum value of J_F factor of the HCF rod in rectangular arrangement is 1.6 % higher than that in triangular arrangement, and the minimum value is 11 % lower than that in the triangular arrangement.
(5) Compared with the rectangular arrangement, the triangular arrangement shows greater advantages in flow and heat transfer characteristics. However, it is necessary to further consider the influence of heat flux distribution to avoid the fracture caused by excessive temperature difference on the fuel rod surface.

CRediT authorship contribution statement

Renwei Tang: Conceptualization, Data curation, Formal analysis, Funding acquisition, Investigation, Methodology, Software, Validation, Visualization, Writing – original draft. **Hangbin Zhao:** Data curation,

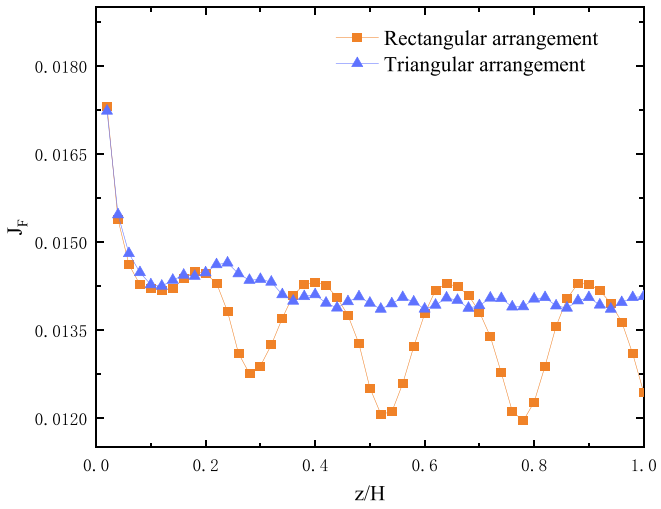

Fig. 25. Comparison of J_F value.

Funding acquisition, Methodology, Project administration, Resources, Supervision, Writing – review & editing. **Nailiang Zhuang:** Formal analysis, Methodology, Resources, Writing – review & editing. **Xiaobin Tang:** Software, Validation, Writing – review & editing.

Declaration of competing interest

The authors declare that they have no known competing financial interests or personal relationships that could have appeared to influence the work reported in this paper.

Data availability

No data was used for the research described in the article.

Acknowledgements

This research is jointly supported by the National Natural Science Foundation of China (Grant No. 12205152), the Natural Science Foundation of Jiangsu Province (Grant No. BK20220904), the Fundamental Research Funds for the Central Universities (Grant No. NS2021060 and Grant No. NJ2022019-1) and the Postgraduate Research & Practice Innovation Program of NUAA (Grant No. xcxjh20231506).

References

Ageenkov, V.I., Volkov, V.S., Solonin, M.I., Garusov, E.A., Zvezdkin, V.S., Konoplev, K.S., et al., 2002. Parameters and technology for fabricating PIK reactor fuel elements. At. Energ. 92 (6), 468–474.

Chen, J., Zhang, D., Song, P., Wang, X., Wang, S., Liang, Y., et al., 2018. CFD investigation on thermal-hydraulic behaviors of a wire-wrapped fuel subassembly for sodium-cooled fast reactor. Ann. Nucl. Energy 113, 256–269.

Conboy, T.M., McKrell, T.J., Kazimi, M.S., 2013. Experimental investigation of hydraulics and transverse mixing for helical-cruciform fuel rod assemblies. Nucl. Technol. 182 (3), 259–273.

Conboy, T.M., Mckrell, T.J., Kazimi, M.S., 2014. Evaluation of helical-cruciform fuel rod assemblies for high-power-density LWRs. Nucl. Technol. 188 (2), 139–153.

Cong, T., Zhang, Q., Zhu, J., Xiao, Y., Guo, H., Gu, H., 2023. Transverse mixing characteristics of single-phase flow in the helical cruciform fuel assembly. Ann. Nucl. Energy 180, 109427.

Fang, Y., Qin, H., Wang, C., Zhou, L., Zhang, J., Zhang, D., et al., 2021. Numerical investigation on thermohydraulic performance of high temperature hydrogen in twisted rod channels. Ann. Nucl. Energy 161, 108434.

Gabrielli, R.A., Herdrich, G., 2015. Review of nuclear thermal propulsion systems. Prog. Aerosp. Sci. 79, 92–113.

Han, Z.Z.J., Wang, M., Tian, W., Su, G., Qiu, S., 2022. Analysis of thermodynamic property, flow and heat transfer model of hydrogen in NTP System. At. Energy Sci. Technol.. 56(7):9.

Jiang, D., Zhang, D., Tian, W., Qiu, S., Su, G.H., 2023. Numerical study on transverse mixing characteristics of flow sweeping in helical cruciform rod bundle. Appl. Therm. Eng. 222, 119935.

Liu, L., Wang, S., Bai, B.F., 2017. Thermal-hydraulic comparisons of 19-pin rod bundles with four circular and trapezoid shaped wire wraps. Nucl. Eng. Des. 318, 213–230.

Malone, J., Totemeier, A., Shapiro, N., Vaidyanathan, S., 2012. Lightbridge corporation's advanced metallic fuel for light water reactors. Nucl. Technol. 180 (3), 437–442.

Palomares, K., Howard, R., Steiner, T., 2020. Assessment of near-term fuel screening and qualification needs for nuclear thermal propulsion systems. Nucl. Eng. Des. 367, 110765.

Saha, S.K., Ranjan, H., Emani, M.S., Bharti, A.K., 2020. Performance Evaluation Criteria in Heat Transfer Enhancement.

Taylor, M.F. 1970. Experimental local heat-transfer and average friction data for hydrogen and helium flowing in a tube at surface temperatures up to 5600 R (Issue November).

Xiao, Y., Fu, J., Zhang, Q., Zhao, H., Gu, H., 2021. Development of a flow sweeping mixing model for helical fuel rod bundles. Ann. Nucl. Energy 160, 108428.

Zhang, Q., Cong, T., Xiao, Y., Li, J., Zeng, C., Gu, H., 2022. Comparison on the thermal–hydraulic characteristics of wire-wrapped fuel and helical cruciform fuel by numerical simulation. Ann. Nucl. Energy 177, 109291.

Zhao, H., Gu, H., Liu, M., et al., 2022. Numerical investigation of transverse flow and turbulent mixing in a helical cruciform fuel bundle. Ann. Nucl. Energy 169, 108944.

Zhao, P.H., Liu, J.M., Ge, Z.H., Wang, X., Cheng, X., 2017. CFD analysis of transverse flow in a wire-wrapped hexagonal seven-pin bundle. Nucl. Eng. Des. 317, 146–157.